Ligand−Receptor Interactions in Chains of Colloids: When Reactions Are Limited by Rotational Diffusion†

Nam-Kyung Lee,‡ Albert Johner,§ Fabrice Thalmann,§ Laetitia Cohen-Tannoudji,|| Emanuel Bertrand,|| Jean Baudry,|| Jérôme Bibette,|| and Carlos M. Marques*,§

Department of Physics, Institute of Fundamental Physics, Sejong University, 143-747, Seoul, Institut Charles Sadron CNRS UPR 22 and ULP, 6 rue Boussingault, F-67083 Strasbourg Cedex, France, and Laboratoire Colloïdes et Matériaux Divisés, ESPCI, ParisTech, Université Pierre et Marie Curie, CNRS UMR 7612, 10 rue Vauquelin, Paris F-75231 Cedex 05, France

Received June 4, 2007. In Final Form: August 2, 2007

We discuss the theory of ligand receptor reactions between two freely rotating colloids in close proximity to one other. Such reactions, limited by rotational diffusion, arise in magnetic bead suspensions where the beads are driven into close contact by an applied magnetic field as they align in chainlike structures. By a combination of reaction−diffusion theory, numerical simulations, and heuristic arguments, we compute the time required for a reaction to occur in a number of experimentally relevant situations. We find in all cases that the time required for a reaction to occur is larger than the characteristic rotation time of the diffusion motion τ_{rot}. When the colloids carry one ligand only and a number n of receptors, we find that the reaction time is, in units of τ_{rot}, a function simply of n and of the relative surface α occupied by one reaction patch $\alpha = \pi r_C^2/(4\pi r^2)$, where r_C is the ligand receptor capture radius and r is the radius of the colloid.

1. Introduction

Ligand receptor pairs build lock-and-key complexes through the formation of specific noncovalent bonds.[1] They play a crucial role in cell adhesion events that allow the communication, proliferation, differentiation, and migration of cells.[2] The quantitative understanding and control of the molecular recognition mechanisms is an important scientific challenge, not only in the fields of molecular and cell biology but also for immunodiagnosis,[3] a diagnosis of disease based on the detection of antigen−antibody reactions in the blood serum.

Immunochemistry is often based on the precipitation of large complexes made of antibodies and antigens.[4] For instance, if an antigen has two different epitopes binding to two antibodies A and B, to reveal the presence of the antigen, one mixes the sample to be tested with particles grafted with A and B. One usually distinguishes between homogeneous and heterogeneous immunoassays. The homogeneous assay, an old, well-established technique, is made by simultaneously mixing the three components and by monitoring the formation of small clusters with changes in the scattered light. It is currently the simplest and most straightforward test, with several hundred different tests being available for practitioners. In contrast to homogeneous tests, heterogeneous assays comprise several steps of mixing and rinsing; they achieve a much better sensitivity. The sensitivity of homogeneous assays is generally limited by the poor control of the composition of the physiological sample to test, which may contain many adherent proteins. This brings about unwanted nonspecific adhesion between colloids, the false positives, which is usually prevented by coating the beads with a protective layer that in turn reduces the specific adhesion to be detected, the false negatives. A possible strategy for improving test sensitivity consists of enhancing the specific adhesion rate by enforcing some degree of local organization among colloids. For instance, ultrasonic standing wave patterns have been used[5] for this purpose, concentrating the colloids near the nodes, with a resulting 2 orders of magnitude increase in sensitivity.

Recently, Bibette et al. discovered that the combined use of magnetic fields and specially designed magnetic colloids provided unique control of the spatial arrangement of the particles.[6] Under a suitable applied magnetic field, the magnetic beads arrange into linear chains with a finely controlled, adjustable relative spacing. When the field is switched off, the beads reversibly disperse if no binding has occurred. The speed of assembly and disassembly is faster in many cases than the characteristic binding rates of functionalized particles, thus offering an unmatched tool to probe the adhesion kinetics with fast time resolution. Kinetic studies from organized particles functionalized with streptavidin and biotin are very promising. They allow one to test the kinetics of biorecognition complex formation as a function of the relevant physical parameters.

Experimentally, the reaction kinetics is better studied when most colloids of the magnetic chain carry the receptors but only a few colloids bear a single ligand. Under these conditions, the formation of colloid aggregates larger than dimers is prevented, and the time evolution of dimer formation can been monitored by light diffusion techniques. The parameters associated with the ligands and the receptors involved in the reaction can now be well controlled, allowing for tuning the number or receptors or ligands per colloid or the spacer length and rigidity. The theoretical challenge that we thus face is to directly relate the measured reaction rates and the molecular ligand receptor

† Part of the Molecular and Surface Forces special issue.

‡ Sejong University.

§ Institut Charles Sadron.

|| Université Pierre et Marie Curie.

(1) Alberts, B.; Johnson, A.; Lewis, J.; Raff, M.; Roberts, K.; Walter, P. *Molecular Biology of the Cell*, 4th ed.; Garland: New York, 2002.

(2) Bongrand, P. *Rep. Prog. Phys.* **1999**, *62*, 921−968.

(3) Price, C. P.; Newman, D. J. *Principles and Practice of Immunoassay*; Stockton Press: New York, 1991.

(4) Baudry, J.; Bertrand, E.; Lequeux, N.; Bibette, J. *J. Phys.: Condens. Matter* **2004**, *16*, R469−R480.

(5) Thomas, N. E.; Coakley, W. T. *Ultrasound Med. Biol.* **1996**, *22*, 1277−1284.

(6) Baudry, J.; Rouzeau, C.; Goubault, C.; Robic, C.; Cohen-Tannoudji, L.; Koenig, A.; Bertrand, E.; Bibette, J. *Proc. Natl. Acad. Sci. U.S.A.* **2006**, *103*, 16076−16078.

10.1021/la701639n CCC: $37.00
Published on Web 10/23/2007 PAGE EST: 11.7

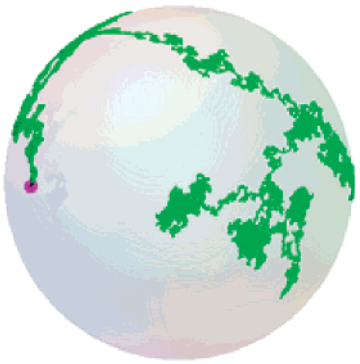

Figure 1. Illustration of the rotational diffusion trajectory of the biotin position over the angle configuration space.

parameters. Related problems have been tackled by scientists studying bioadhesion in general.[7−10] Our contribution not only clarifies some of the open questions related to the underlying dimensionality of reaction diffusion problems dealing with surface-bound ligands or receptors[11] but also provides a convenient framework for interpreting the role of rotational diffusion in colloidal reaction kinetics. Theoretically, we adapt to this geometry a formalism introduced for polymers by Doi[12−14] and de Gennes[15] and used by us in the context of specific adhesion.[16−19]

In this article, we consider theoretically and numerically the reaction kinetics of ligand−receptor binding between two adjacent colloids in a chain. In the next section, we compute analytically dimerization rates for the two limiting cases where one bead carries a single ligand and the other bead is either fully covered by receptors or carries only one receptor. We also provide qualitative arguments for understanding the dependence of the reaction time on the different relevant parameters. Section 3 presents numerical simulation results for the more general case where one colloid carries an arbitrary number of receptors. The last section discusses the experimental relevance of these results and presents directions for future developments.

2. Specific Reactions between Rotating Colloids

We consider two neighboring colloidal beads of identical radius r that are kept close to one another. Each of the beads is free to undergo rotational Brownian motion as displayed in Figure 1 with the usual rotational diffusion coefficient $D_r = \tau_{rot}^{-1} = k_B T/(8\pi\eta r^3)$ that has inverse dimensions of time, where k_B is the Boltzmann constant, T is the absolute temperature, and η is the solvent viscosity.

2.1. Reaction between One Colloid Carrying a Single Ligand and One Colloid Saturated with Receptors. In this section, we tackle the simplest reaction geometry where one bead, say bead number one on the left of Figure 2, carries one ligand and bead number two is saturated with the complementary receptors. The only relevant variable is thus the orientation of bead number one, which can be described with respect to the axis connecting the centers of the colloids by the usual two angular variables (θ, ϕ). We assume axisymmetric reactions for which the reaction geometry is independent of the angle, ϕ. A reaction is assumed to occur provided that θ is smaller than the capture angle, θ_C. This angle also defines the so-called capture patch with radius $r_C = \sqrt{2}r(1 - \cos\theta_C)^{1/2}$.

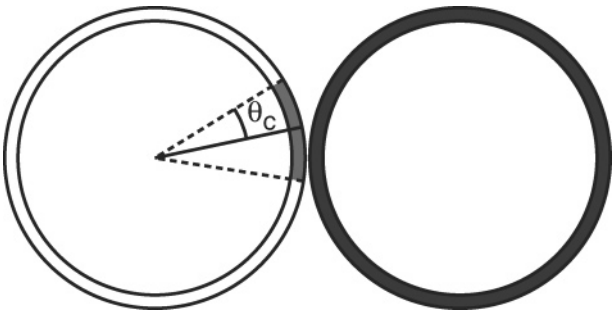

Figure 2. Two colloids facing each other. The left colloid carries one ligand, and the right colloid is fully covered by receptors. A reaction occurs within the reaction cone $\theta \le \theta_C$, which corresponds visually to physical contact between the right colloid and the shaded angular section on the left colloid.

We consider the probability distribution $\Psi(\theta, \phi; t)$ describing the orientation of bead number one at time t and in particular the projected probability for axisymmetric systems $\psi(\theta, t) = \int_0^{2\pi} d\phi\ \Psi(\theta, \phi; t)$. In the absence of reactions, the equilibrium probability distribution is independent of the angular position of the bead and reads simply $\psi^{eq}(\theta, t) = {}^1/_2$. All quantities $f(\theta)$ are normalized such that $\int_0^\pi \sin\theta\ d\theta\ f(\theta) = 1$. In the presence of reactions, the probability distribution $\psi(\theta, t)$ obeys a diffusion reaction equation of the form

$$\frac{\partial\psi(\theta, t)}{\partial t} - D_r\nabla_\theta^2\psi(\theta, t) = -Q(\theta)\ \psi(\theta, t) \qquad (1)$$

with ∇_θ^2 being the θ component of the angular Laplace operator and $Q(\theta)$ being a reaction operator given by the sink function $Q(\theta) = q$ if $\theta \le \theta_C$ and $Q(\theta) = 0$ otherwise. In the limit of very fast local reactions $\theta \to \infty$, the reaction operator on the right-hand side of eq 1 can be replaced by the boundary condition $\psi(\theta, t) = 0$ for $\theta \le \theta_C$. For convenience and without a loss of generality, D_r is set equal to unity in the following text.

Under most relevant experimental conditions, the reaction kinetics is probed by some measure of the survival probability, $\phi(t)$ (i.e., the fraction of particles that have not reacted at time t after the particles have been brought into intimate contact with each other, $\phi(t) = \int_0^\pi \sin\theta\ d\theta\ \psi(\theta, t)$). Because the forces that bring the particles together do not bias their orientation, eq 1 obeys the initial condition $\psi(\theta, t = 0) = \psi^{eq} = {}^1/_2$.

The solution of the reaction diffusion equation (eq 1) with the prescribed boundary and initial conditions can be written as

$$\psi(\theta, s) = \frac{1}{2s}\left(1 - \frac{P_{\nu(s)}(-\cos\theta)}{P_{\nu(s)}(-\cos\theta_C)}\right) \qquad (2)$$

where $\psi(\theta, s) = \int_0^\infty dt\ \psi(\theta, t)\exp\{-st\}$ is the Laplace transform of the probability distribution, $\nu(s)(\nu(s) + 1) = -s$, and P_ν is the Legendre function of the first kind.[20] Equation 2 holds outside the reaction well $\theta_C \le \theta \le \pi$. We show in Figure 3 the time evolution of the probability distribution, $\psi(\theta, t)$, obtained from the numerical inverse Laplace transformation of eq 2 by the

(7) Shoup, D.; Lipari, G.; Szabo, A. *Biophys. J.* **1981**, *36*, 697−714.
(8) Shoup, D.; Szabo, A. *Biophys. J.* **1982**, *40*, 33−39.
(9) Zhu, C. *J. Biomech.* **2000**, *33*, 23−33.
(10) Nag, A.; Dinner, A. R. *Biophys. J.* **2006**, *90*, 896−902.
(11) Chesla, S. E.; Selvaraj, P.; Zhu, C. *Biophys. J.* **1998**, *75*, 1553−1572.
(12) Doi, M. *Chem. Phys.* **1975**, *9*, 455−466.
(13) Doi, M. *Chem. Phys.* **1975**, *11*, 115−121.
(14) Doi, M. *Chem. Phys.* **1975**, *11*, 107−113.
(15) Degennes, P. G. *J. Chem. Phys.* **1982**, *76*, 3316−3321.
(16) Jeppesen, C.; Wong, J. Y.; Kuhl, T. L.; Israelachvili, J. N.; Mullah, N.; Zalipsky, S.; Marques, C. M. *Science* **2001**, *293*, 465−468.
(17) Moreira, A. G.; Jeppesen, C.; Tanaka, F.; Marques, C. M. *Europhys. Lett.* **2003**, *62*, 876−882.
(18) Moreira, A. G.; Marques, C. M. *J. Chem. Phys.* **2004**, *120*, 6229−6237.
(19) Likthman, A. E.; Marques, C. M. *Europhys. Lett.* **2006**, *75*, 971−977.
(20) Gradshteyn, I. S.; Ryzhik, I. M.; Jeffrey, A.; Zwillinger, D. *Table of Integrals, Series, and Products*, 6th ed.; Academic Press: New York, 2000.

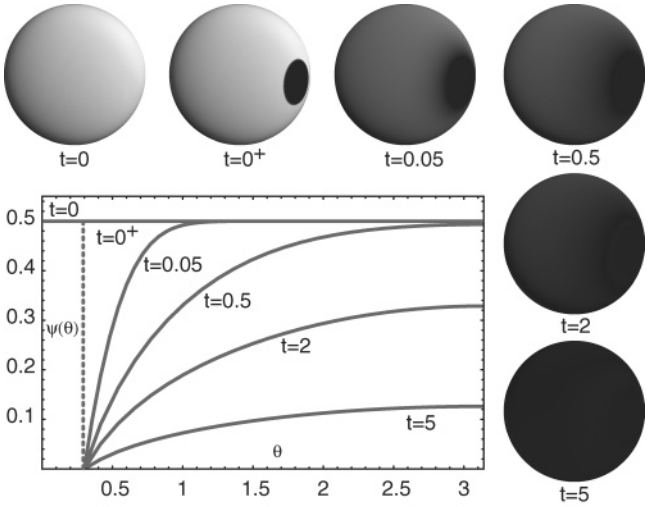

Figure 3. Evolution of the probability distribution $\psi(\theta, t)$ before and after the reaction has started. Times are given in units of $\tau_{rot} = D_r^{-1}$. The extent of the reaction well is given here by $\theta_C = 0.3$ or a relative capture surface $\alpha = \pi r_C^2/(4\pi r^2) = (1 - \cos 0.3)/2 = 0.022$. In the 3D representation, the gray level of the spheres surface is proportional to $\psi(\theta, t)$.

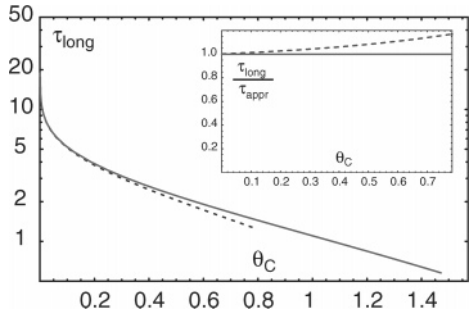

Figure 4. Longest relaxation time τ_{long} (−) of the probability distribution $\psi(\theta, t)$ as a function of the capture angle θ_C and the approximated value τ_{appr} (---) given in the text. The relative value τ_{long}/τ_{appr} is given in the inset.

Stenhfest method.[21] We also give in Appendix A an equivalent eigenmode expansion for the time evolution of the probability distribution.

The reaction starts by instantaneously collecting all particles within the capture radius, consistent with the assumed limit of very fast local reactions, $q \to \infty$. The particles outside the capture radius follow free rotational diffusion until they hit the reaction well. The trajectories of these particles started outside the capture radius and diffused into the well region. Such trajectories last a characteristic time τ_{rot}, but a fraction of the particles miss the reaction zone. That fraction increases as the capture radius decreases, implying that the longest decay time τ_{long} of the probability distribution is larger than τ_{rot}. This can be computed from the smallest pole of eq 2 by solving $P_{\nu(-1/\tau_{long})}(-\cos\theta_C) = 0$ in units of τ_{rot}. The numerical result is displayed in Figure 4 as a function of the capture angle, θ_C. In the relevant limit of small capture radius $r_C \ll r$, the inset of Figure 4 shows also that the longest relaxation time τ_{long} can be well approximated by

$$\frac{1}{\tau_{long}} \simeq \frac{1}{\tau_{appr}} = -\frac{1}{\tau_{rot}}\frac{1}{\ln\alpha}\left(1 - \frac{1}{\ln\alpha}\right) \qquad (3)$$

where $\alpha = (1 - \cos\theta_C)/2 = \pi r_C^2/(4\pi r^2)$ is the relative capture surface. The approximation τ_{appr} holds to less than 16% deviation

(21) Mallet, A. *Numerical Inversion, Mathematica Package*, 2000.

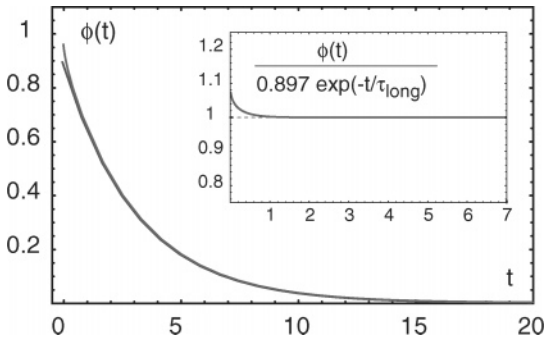

Figure 5. Survival probability $\phi(t)$ for $\theta_C = 0.3$ or $\alpha = 0.022$. In this case, $\tau_{long} = 3.13\tau_{rot}$. The plot and the inset show that an exponential decay function well describes $\phi(t)$ for most of the time domain. The amplitude of the exponential function is computed from the eigenvalue method presented in Appendix A.

up to $\theta_C = \pi/4$ ($\alpha = 0.15$). For even smaller angles, one can simply write $\tau_{appr} = \tau_{rot} \ln \alpha e$ with $\ln e = 1$, which is accurate to better than 16% up to $\theta_C = \pi/8$ ($\alpha = 0.04$).

The Laplace transform of the survival probability $\phi(s) = \int_{\theta_C}^{\pi} \sin\theta \, d\theta \, \psi(\theta, s)$ can now be computed from eq 2

$$\phi(s) = \frac{1}{s}\left(\frac{1 + \cos\theta_C}{2} - \frac{\sin\theta_C}{2P_{\nu(s)}(-\cos\theta_C)}P^{-1}_{\nu(s)}(-\cos\theta_C)\right) \qquad (4)$$

where P_ν^{-1} is the associated Legendre function of indices ν and -1. Note that the survival probability $\phi(s)$ and the distribution function $\psi(\theta, s)$ have the same pole and their inverse Laplace transforms $\phi(t)$ and $\psi(\theta, t)$ both asymptotically display an exponential decay of $\sim\exp(-t/\tau_{long})$, with the same decay time τ_{long}. Figure 5 shows the time evolution of $\phi(t)$ obtained by a numerical inverse Laplace transform. As the Figure shows, an exponential function well describes the time evolution of the survival probability, except at very short times. Appendix A discusses the value of the amplitude associated with the exponential decay. In practice, experiments that cannot resolve very short time scales $t \ll \tau_{long}$ will not detect any differences from exponential behavior, and the reaction will appear to be a first-order reaction.

When the full time evolution of the reaction kinetics is not experimentally available, it might still be possible to access some moment of the survival probability, $\phi(t)$. The simplest quantity that is usually available is the average decay time

$$\langle\tau\rangle = \int_0^\infty \phi(t)\, dt = \lim_{s\to 0} \phi(s) = -\ln(\alpha e) + \alpha \qquad (5)$$

in units of τ_{rot}. Note that this is a less universal quantity than the longest decay time τ_{long} because it depends on the initial state of the system. However, in the relevant limit where the capture surface is small, $\alpha \ll 1$, the two quantities coincide, $\langle\tau\rangle \simeq \tau_{long}$.

2.2. Reaction between One Colloid Carrying a Single Ligand and Two Neighboring Colloids Saturated with Receptors. In magnetic bead experiments, each colloid has two neighbors, which reduces the time needed for a reaction to occur. The probability distribution obeys a rotational diffusion equation similar to eq 1 but with different boundary conditions $\psi(\theta, t) = 0$ for $0 \le \theta \le \theta_C$ and $\pi \ge \theta \ge \pi - \theta_C$ (Figure 6). In this case, the solution can be written as

$$\psi(\theta, s) = \frac{1}{2s}\left(1 - \frac{P_{\nu(s)}(-\cos\theta) + P_{\nu(s)}(\cos\theta)}{P_{\nu(s)}(-\cos\theta_C) + P_{\nu(s)}(\cos\theta_C)}\right) \qquad (6)$$

A procedure parallel to that of the previous section gives the

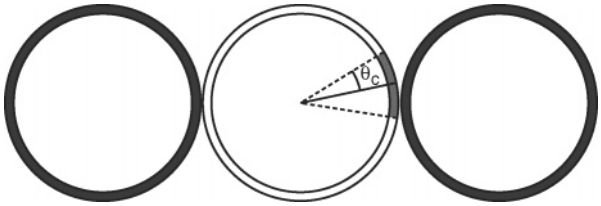

Figure 6. Three colloids facing each other. The middle colloid carries one ligand, and the right and left colloids are fully covered with receptors. A reaction occurs within the reaction cone $0 \le \theta \le \theta_C$ and $\pi \ge \theta \ge \pi - \theta_C$, which corresponds visually to physical contact between the right or left colloid and the shaded angular section on the middle colloid.

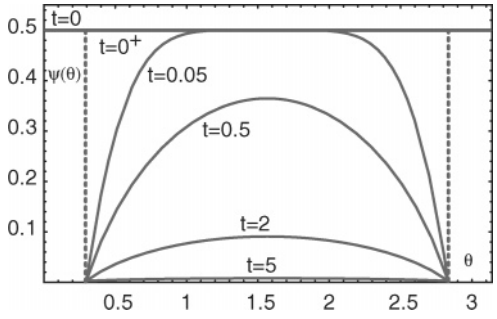

Figure 7. Evolution of probability distribution $\psi(\theta, t)$ before and after the reaction has started. Times are given in units of D_r^{-1}. There are two reaction wells at $0 \le \theta \le \theta_C = 0.3$ and $\pi \ge \theta \ge \theta_C = \pi - 0.3$ with a total relative capture surface of $\alpha = 2\pi r_C^2/(4\pi r^2) = 2(1 - \cos 0.3)/2 = 0.044$.

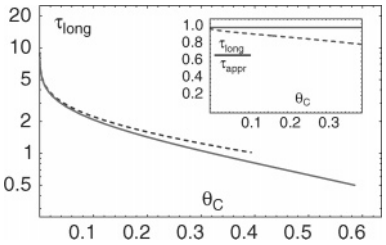

Figure 8. Longest relaxation time τ_{long} (−) as a function of capture angle θ_C and approximated value τ_{appr} (---) given in the text. The relative value τ_{long}/τ_{appr} is given in the inset.

main relevant physical quantities. The evolution of the probability distribution is presented in Figure 7. The presence of the two reaction sinks around the two poles leads to a faster evolution of the probability distribution, as can be seen by directly comparing Figures 7 and 3.

The longest relaxation time τ_{long} is now given by the smallest pole of eq 6, and it can be computed by solving $P_{\nu(-1/\tau_{long})}(-\cos\theta_C) + P_{\nu(-1/\tau_{long})}(\cos\theta_C) = 0$. Figure 8 shows the dependence of τ_{long} on the reaction angle θ_C and how it compares to the small-angle approximation

$$\frac{1}{\tau_{long}} \simeq \frac{1}{\tau_{appr}} = -\frac{1}{\tau_{rot}} \frac{2}{\ln[\alpha(1-\alpha)]}\left(1 - \frac{2}{\ln[\alpha(1-\alpha)]}\right) \quad (7)$$

Note that the relaxation time for this configuration with two sinks is, in the limit of a small capture radius, close to half of the longest relaxation time of the configuration with a single sink. Figure 9 compares the values of the two relaxation times as a function of the capture angle. As expected, there is almost a factor of 2 between the two relaxation times in the limit of a small capture radius, indicating a negligible correlation between the reaction events at both poles. Note however that the convergence is slow (∼1/ln α).

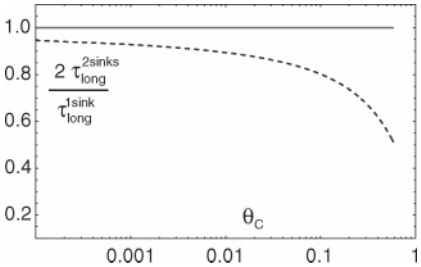

Figure 9. Ratio of the two longest relaxation times for the configurations with one sink and two sinks. Relaxation time τ_{long}^{2sinks} of the configuration with two sinks is in the limit of very small capture angles close to half of τ_{long}^{1sink}, the relaxation time with one sink. Note, however, the slow (1/ln α) convergence.

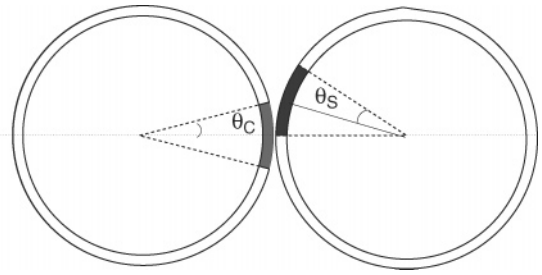

Figure 10. Two colloids within the reaction range. The left colloid, colloid 1, carries one ligand, and the right colloid, colloid 2, bears one receptor. A reaction occurs within the reaction cone of $0 \le \theta_1 \le \theta_C$ and $0 \le \theta_2 \le \theta_S$.

One also expects in this case an almost pure exponential relaxation of the survival probability $\phi(t)$. Appendix B presents an eigenmode expansion of both the probability distribution $\psi(\theta, t)$ and the survival probability $\phi(t)$; it also provides the values of the amplitudes of the relaxation modes. For comparison, the value of the amplitude for the case of $\theta_C = 0.3$ is 0.339, to be compared with the value of 0.897 shown in Figure 5 for one sink. However, most of the relevant situations correspond to vanishingly small capture angles, and the amplitudes of cases with one or two sinks can be taken as unity, with the main difference between the expected decays residing in the relaxation times. It can also be shown in this case that the average reaction time is given by

$$\langle\tau\rangle = -\frac{1}{2}\ln\frac{\alpha}{1-\alpha} + 2\alpha - 1 \quad (8)$$

2.3. Reaction between One Colloid Carrying a Single Ligand and One Colloid Carrying a Single Receptor. We consider in this section a reaction configuration at the opposite limit in the range of surface coverage: as before, bead number one carries one ligand, but bead number two carries only one complementary receptor (Figure 10). The reaction geometry now has a larger intrinsic dimension, and the orientation of both beads needs to be specified here. We choose the two sets of angular variables (θ_1, ϕ_1) and (θ_2, ϕ_2) measured with respect to the axis connecting the centers of the two spherical particles. We further assume axisymmetric reactions for which the reaction geometry is independent of angles ϕ_1 and ϕ_2. A reaction is assumed to occur provided that θ_1 is smaller than capture angle θ_C and θ_2 is smaller than capture angle θ_S. Recall that these angles also define capture patch radii $r_C = \sqrt{2}r(1 - \cos\theta_C)^{1/2}$ and $r_S = \sqrt{2}r(1 - \cos\theta_S)^{1/2}$.

We consider probability distributions $\Psi_1(\theta_1, \phi_1; t)$ and $\Psi_2(\theta_2, \phi_2; t)$ describing the orientation of the beads at time t and, in particular, projected probabilities for axiosymmetric systems $\psi_1(\theta_1, t) = \int_0^{2\pi} d\phi_1 \Psi_1(\theta_1, \phi_1; t)$ and $\psi_2(\theta_2, t) =$

$\int_0^{2\pi} d\phi_2 \Psi(\theta_2, \phi_2; t)$. In the absence of reactions, the equilibrium probability distributions are independent of the angular positions of the beads and read simply $\psi_1^{eq}(\theta_1) = \psi_2^{eq}(\theta_2) = 1/2$. In the presence of the reaction between the two beads, joint probability $\psi(\theta_1, \theta_2; t)$ obeys the reaction diffusion equation

$$\frac{\partial \psi(\theta_1, \theta_2; t)}{\partial t} - \nabla^2_{\theta_1} \psi(\theta_1, \theta_2; t) - \nabla^2_{\theta_2} \psi(\theta_1, \theta_2; t) = -Q(\theta_1, \theta_2)\, \psi(\theta_1, \theta_2; t) \quad (9)$$

with reaction function $Q(\theta_1, \theta_2) = q$ if ($0 \le \theta_1 \le \theta_C$ and $0 \le \theta_2 \le \theta_S$) and $Q = 0$ otherwise. When the initial distribution is the equilibrium distribution, $\psi^{eq}(\theta_1,\theta_2) = \psi_1^{eq}(\theta_1)\, \psi_2^{eq}(\theta_2) = 1/4$, the solution of the above reaction diffusion equation can be formally written as

$$\psi(\theta_1, \theta_2; t) = \frac{1}{4} - q \int_0^t dt' \int_0^{\theta_C} \sin\theta_1' \, d\theta_1' \int_0^{\theta_S} \sin\theta_2' \, d\theta_2' \, \psi(\theta_1', \theta_2'; t')\, G_0(\theta_1, \theta_1'; t - t')\, G_0(\theta_2, \theta_2'; t - t') \quad (10)$$

with $G_0(\theta_1, \theta_1'; t)$ being the single-particle propagators of the free diffusion case, as discussed in Appendix C. This formal solution simply states that the probability distribution at time t is the equilibrium distribution depleted from all of those trajectories that have visited the reaction well at any previous time t'. The bare propagators G_0 in eq 10 are smooth functions that are independent of the reaction sink positions, unlike the probability distribution ψ that has a much lower value (vanishingly small when $q \to \infty$) inside the sink and strong gradients nearby when the reaction cones are small, $\theta_C \ll 1$ and $\theta_S \ll 1$. In the first approximation, θ_1' and θ_2' can then be set equal to zero in the expression for G_0. The Laplace transform of the survival probability $\phi(s) = \int_0^{\pi} \sin\theta_1' \, d\theta_1' \int_0^{\pi} \sin\theta_2' \, d\theta_2' \, \psi(\theta_1', \theta_2'; s)$ can be computed from eq 10, leading to

$$\phi(s) = \frac{h(s)}{1 + s h(s)} \quad (11)$$

where $h(s)$ is the Laplace transform of relaxation function $h(t)$. In the limit of instantaneous reaction ($q \to \infty$), the relaxation function is given by

$$h(t) = \frac{\int_0^{\theta_C} \sin\theta \, d\theta \, G_0(\theta, 0; t) \int_0^{\theta_S} \sin\theta \, d\theta \, G_0(\theta, 0; t)}{\int_0^{\theta_C} \sin\theta \, d\theta \, \psi^{eq} \int_0^{\theta_S} \sin\theta \, d\theta \, \psi^{eq}} - 1 \quad (12)$$

The longest relaxation time of the survival probability, τ, is given by the smallest pole in eq 11, which is the smallest solution of $1 + s h(s) = 0$. The existence of such a pole also shows that the survival probability has a long-time exponential decay, $\phi(t) \approx \exp\{-t/\tau_{long}\}$, that can be effectively interpreted in this limit as resulting from first-order kinetics. Here it is more convenient to calculate the average relaxation time $\langle\tau\rangle = \int_0^{\infty} dt \, h(t)$ for an initially homogeneous distribution $\psi(\theta_1, \theta_2; t = 0) = 1/4$. Because we are interested in the limit of small reaction patches, we can approximate the full angle-dependent propagator by its projection in a flat 2D plane as $G_{2d}(\theta, 0; t) = 1/(4\pi D_r t) \exp\{-2(1 - \cos\theta)/(4D_r t)\}$. In this limit, one can analytically perform the integrations over the reaction cones to obtain

$$\langle\tau\rangle = \tau_{rot} \frac{4r^2}{r_C r_S} \left[\left(\frac{r_C}{r_S} + \frac{r_S}{r_C} \right) \ln\left(\frac{r_C}{r_S} + \frac{r_S}{r_C} \right) + \left(\frac{r_S}{r_C} - \frac{r_C}{r_S} \right) \ln\left(\frac{r_C}{r_S} \right) \right] \quad (13)$$

The value of the average time $\langle\tau\rangle$ is insensitive to a permutation between r_S and r_C as required by the symmetry of the problem. The situation where $r_C = r_S$ is of particular interest. In this symmetric limit, the average reaction time reduces to the simple expression

$$\langle\tau\rangle = \tau_{rot}(8 \ln 2) \frac{r^2}{r_C^2} = \tau_{rot} \frac{2 \ln 2}{\alpha} \quad (14)$$

The reaction time in this configuration increases in inverse proportion to the relative capture surface $\alpha = \pi r_C^2/(4\pi r^2)$, which is a much stronger dependence than the logarithmic variation obtained when one of the beads is fully covered with receptors.

2.4. Beyond Numbers: Qualitative Arguments to Understand the main Contributions to the Reaction Times. In the previous sections, we derived expressions for mean reaction time $\langle\tau\rangle$ and for asymptotic decay time τ_{long} in a variety of situations. The goal of this paragraph is to revisit our results from a more qualitative point of view in order to distinguish the general features of the reaction diffusion behavior, such as those associated with intrinsic dimensionality or the number of degrees of freedom of the configurational space, from the specific features associated, for instance, with the spherical geometry or with the details of the precise distribution of ligands and receptors on the colloidal surface.

We found that the asymptotic behavior of our expressions for $\langle\tau\rangle$ or τ_{long} results from simple geometrical considerations, among which the dimension d of the configuration space plays a prominent role. The case of a spherical bead bearing a single ligand and surrounded by one or two beads saturated with receptors belongs to the $d = 2$ situation, known as marginal and characterized by an extra logarithmic dependence on the size of the system. The case of a bead bearing a single ligand and surrounded by one or more beads bearing only a few receptors has an intrinsic dimension, $d = 4$; here also scaling trends are derived from the geometrical features of the Brownian exploration in configurational space. In contrast, the curvature of the configuration space plays a lesser role.

As far as the importance of the distribution and number n of capture patches around the beads is concerned, further arguments for understanding our results come from the analogy that can be drawn between the classical electrostatics on the one hand and the reaction diffusion dynamics of particles evolving in a flat Euclidean space on the other hand. These are the geometric arguments and electrostatic analogies that we discuss below.

2.4.1. Geometric Arguments. Let us first consider a particle that explores a sphere of radius r, trying to find a patch of radius r_C, which is small compared with r. We adopt a coarse-grained description of the Brownian trajectory, mapping it onto a random walk, with an elementary time step τ_{patch} and a finite number N of different accessible positions. The coarse-grained time step scales naturally as $\tau_{patch} = r_C^2/(2D_t)$, with D_t being the translational diffusion coefficient of the reference point along the surface of a sphere where both quantities are dimensionally related by $D_t = D_r r^2$. The number of sites N is given by the minimal number of patches necessary to cover the whole sphere: $N = 4\pi r^2/\pi r_C^2$. Note that $N = \alpha^{-1}$, with α being the ratio of the capture area to the total area. A classical result for bidimensional random walks[22,23] states that the actual number $N_{\neq}$ of different sites visited by a walker after a time interval t is given by

(22) Montroll, E. W.; West, B. J. In *Fluctuation Phenomena*; Studies in Statistical Mechanics; Lebowitz, J. L., Montroll, E., Eds.; North-Holland: Amsterdam, 1979; Vol. 7.

(23) Bouchaud, J. P.; Georges, A. *Phys. Rep.* **1990**, *195*, 127−293, 321.

$$N_{\neq}(t) \simeq \frac{t}{\tau_{\text{patch}}} \times \frac{1}{\ln\left(\frac{t}{\tau_{\text{patch}}}\right)} \tag{15}$$

Hence, the typical time τ_{typ} needed by a walker starting from a random position to find a particular patch (the capture zone $\mathscr{R}$) among N available positions obeys $N_{\neq}(\tau_{\text{typ}}) \simeq N$. Solving for τ_{typ} leads to

$$\tau_{\text{typ}} = \tau_{\text{patch}} N \ln(N) + \ldots \simeq \tau_{\text{patch}} \frac{4r^2}{r_C^2} \ln\left(\frac{4r^2}{r_C^2}\right) \tag{16}$$

When adapting the above expression to the case of a spherical bead for which $N = \alpha^{-1}$, we finally get

$$\tau_{\text{typ}} = -\tau_{\text{rot}} \ln(\alpha) \tag{17}$$

in agreement with our result eq 3.

By contrast, this logarithmic correction is absent in any dimension equal to or larger than $d = 3$, where $N_{\neq}$ simply scales as $c_d t/\tau_{\text{patch}}$,[22,23] with the constant c_d depending on both the dimension and the connectivity of the network that supports the walk, which we arbitrarily set equal to 1. In the $d = 4$ situation characterizing our two beads with a single ligand−receptor pair, in the symmetric situation $r_C = r_S$ we find that

$$N = \left(\frac{4\pi r^2}{\pi r_C^2}\right)^2 = \frac{1}{\alpha^2} \tag{18}$$

and a repetition of the previous argument with $N_{\neq} = t/\tau_{\text{patch}}$ gives

$$\tau_{\text{typ}} = \tau_{\text{patch}} \frac{16r^4}{r_C^4} = \frac{\tau_{\text{patch}}}{\alpha^2} \tag{19}$$

Introducing the total volume of the configuration space ν_{conf} and of the capture patch ν_{patch}, this geometrical argument gives, in any dimension d equal or larger than 3, $\tau_{\text{typ}} = \tau_{\text{patch}} \nu_{\text{conf}}/\nu_{\text{patch}}$. In the case of two spherical beads, $\tau_{\text{rot}} = 4\tau_{\text{patch}} r^2/r_C^2$, and the relation becomes

$$\tau_{\text{typ}} = \frac{\tau_{\text{rot}}}{\alpha} \tag{20}$$

in agreement with eq 14 up to the numerical value of the prefactor that is not predicted by this approach.

2.4.2. Electrostatic Analogy. Various electrostatic analogies can be drawn with reaction diffusion problems. The key to a useful analogy is to recognize a Poisson equation in the reaction diffusion process and to consider a flat Euclidean configuration space that greatly simplifies the technical difficulty of the problem. Our previous geometrical arguments show that neglecting curvature still allows one to capture the correct leading behavior of the reaction time.

To start with, it is possible to propose an electrostatic analogy for the transient diffusion dynamics of an initial distribution of particle positions; these particles are subsequently absorbed at the boundary (noted $\partial\mathscr{R}$) of the capture zone. In the presence of many capture zones $\mathscr{R}_i$ and starting from a single particle located anywhere outside them, the resolution of the associated electrostatic problem gives the probability p_i that the particle eventually ends its life captured at boundary $\partial\mathscr{R}_i$ of patch $\mathscr{R}_i$. These techniques are known, in the theory of probability, as potential theory.

Conversely, the connection between the electrostatic capacitances of a set of perfect conductors in vacuum and the related reaction−diffusion problem can be used to compute the electrostatic capacitances of arbitrarily shaped conductors from stochastic numerical simulations.[24] Inspired by such connections, we present here an electrostatic analogy for a stationary reaction−diffusion process, which, as we shall see, provides useful predictions for the behavior of a diffusive particle in the presence of many capture zones.

We start with a single small capture disk $\mathscr{R}$ of radius r_C located at the center of a larger 2D flat disk of radius a and we name $\boldsymbol{\rho}$ the vector position of a point, with $\rho = ||\boldsymbol{\rho}||$ being the distance to the center. We suppose that our concentration field $\psi(\boldsymbol{\rho})$ does not show any explicit time dependence. This situation arises when particles are injected at the periphery such as to exactly replace the ones that disappear when hitting the reaction zone. One has to solve the electrostatic problem

$$\Delta[D_t \psi(\boldsymbol{\rho})] = 0 \tag{21}$$

along with the boundary condition $\psi(||\boldsymbol{\rho}|| = r_C) = 0$ with solution

$$D_t \psi(\boldsymbol{\rho}) = \frac{Q}{2\pi} \ln\left(\frac{\rho}{r_C}\right) \tag{22}$$

Here, $V(\boldsymbol{\rho}) = D_t \psi(\boldsymbol{\rho})$ plays the role of potential $V(\boldsymbol{\rho})$, and charge Q is nothing but the *rate* of particles falling into the reaction zone per unit of time (decay rate). We then compute the total number N of particles present in the system:

$$N = 2\pi \int_{r_C}^{a} \boldsymbol{\rho}\, \mathrm{d}\boldsymbol{\rho}\, \psi(\boldsymbol{\rho}) = \frac{Q}{2D_t}\left[a^2 \ln\left(\frac{a}{r_C \sqrt{\mathrm{e}}}\right) + \frac{r_C^2}{2}\right] \tag{23}$$

Mean lifetime τ of a particle is given by the ratio between decay rate Q and total population N:

$$\tau = \frac{N}{Q} \text{ and } \frac{2D_t \tau}{a^2} = \ln\left(\frac{a}{r_C}\right) - \frac{1}{2} + \frac{r_C^2}{2a^2} \tag{24}$$

Ratio $a^2/2D_t$ is the time necessary to diffuse over a length equal to the linear size of the system. Introducing $\tau_{\text{rot}} = a^2/(4D_t)$ and surface ratio $\alpha = \pi r_C^2/\pi a^2$, we get

$$\tau = \tau_{\text{rot}}\left(\ln\left(\frac{a^2}{r_C^2}\right) - 1 + \alpha\right) = -\tau_{\text{rot}}(\ln(\alpha e) - \alpha) \tag{25}$$

Equation 5 is recovered when setting radius a equal to $2r$ (diameter of the bead), and we find in the limit $\alpha \to 0$ that $\tau^{-1} = -\tau_{\text{rot}}^{-1} \ln(\alpha)^{-1}[1 - \ln(\alpha)^{-1}] + O(\ln(\alpha)^{-2})$, similar to eq 3.

At higher dimension d, Coulomb potential V created by (hyper)-spherical charge Q at a distance $\rho = ||\boldsymbol{\rho}||$ from the origin and vanishing at $\rho = r_C$ is

$$V(\boldsymbol{\rho}) = D_t \psi(\boldsymbol{\rho}) = \frac{Q}{(d-2)\sigma_d}\left[\frac{1}{r_C^{d-2}} - \frac{1}{\boldsymbol{\rho}^{d-2}}\right] \tag{26}$$

where σ_d is the (hyper)surface of a unit sphere. Repeating the above argument, we find that total population N, between the reaction patch of radius r_C and an outer boundary of radius a, scales as

(24) Zhou, H. X.; Szabo, A.; Douglas, J. F.; Hubbard, J. B. *J. Chem. Phys.* **1994**, *100*, 3821−3826.

$$N = \int_{r_C}^{a} \mathrm{d}\boldsymbol{\rho}\sigma_d \boldsymbol{\rho}^{d-1}\psi(\boldsymbol{\rho}) = \frac{Q}{D_t d(d-2)}\left[\frac{a^d}{r_C^{d-2}} + r_C{}^2\left(\frac{d}{2}-1\right) - \frac{d}{2}a^2\right] \quad (27)$$

Clearly, in the limit $r_C \ll a$, only the first term contributes. Lifetime τ follows:

$$2D_t\tau = \frac{2}{d(d-2)}\frac{a^d}{r_C^{d-2}} \quad (28)$$

Again introducing $\tau_{rot} = a^2/(4D_t)$, the lifetime arising from the electrostatic analogy is

$$\tau = \tau_{rot}\frac{4}{d(d-2)}\frac{a^{d-2}}{r_C^{d-2}} \quad (29)$$

If $d = 4$ and $\alpha = r_C{}^2/a^2$, then the lifetime becomes

$$\tau = \frac{\tau_{rot}}{2\alpha} \quad (30)$$

in agreement with eq 14, except for the prefactor.

2.4.3. Electrostatics Analogy for Many Reaction Sites. The electrostatic analogy helps us to understand the competition resulting from the presence of many identical reaction zones in the configuration space. The analogy shows that the n reaction zones behave as independent patches when their size decreases, leading to a linear dependence in the number n of the reaction rate $\tau_n^{-1} = n\tau_1^{-1} + ...$, which becomes asymptotically exact in the limit of a vanishing patch size $r_C \to 0$.

The electrostatic analogy predicts the following behavior for the reaction time

$$\tau_n = \frac{\tau_a}{n} + \beta_1\tau_{rot} + \beta_2\tau_{patch} + \beta_3\tau_{patch}\left(\frac{a}{r_C}\right)^{2d-2} \quad (31)$$

with some logarithmic corrections in two dimensions and where $\tau_a = \tau_{rot}a^{d-2}/r_C^{d-2}$. In this expression, the first term represents the leading behavior, the second term is a geometric subleading correction independent of the patch size, the third term is a "universal'' geometric subleading term with a quadratic dependence $r_C{}^2$, and the fourth term is a subleading correction related to the mutual influence of the reaction sites (mutual polarization of the conductors). These numbers β_1, β_2, and β_3 are constant once size a and positions of the patches $\mathscr{P}_i$ are fixed. The fourth term also encompasses the $d = 1$ case, where the presence of a capture patch is dramatic, whatever its size. It competes with the third term for $d = 2$ and can be neglected at higher dimensions.

The corresponding expansion for the reaction rate is

$$\frac{1}{\tau_n} = \frac{n}{\tau_a}\left(1 - \left[\beta_1\frac{n\tau_{rot}}{\tau_a} + \beta_2\frac{n\tau_{patch}}{\tau_a} + \beta_3\frac{n\tau_{patch}}{\tau_a}\frac{a^{2d-2}}{r_C{}^{2d-2}}\right]\right) \quad (32)$$

and strong deviations from linearity are expected as soon as ratio $n\tau_{rot}/\tau_a$ is on the order of unity. We defer the derivation of these results to Appendix D.

For a collection of n patches located in a (hyper)spherical volume of radius a and dimension $d \geq 3$ and in the limit $r_C \to 0$, $\tau_a = \tau_{rot}a^{d-2}/r_C^{d-2}$, clearly dominates the other terms in expression 31, promoting $1/n$ behavior. A numerical illustration of the linearity of τ_n^{-1} with n in the particular case of $d = 4$ is provided in the next section.

Table 1. Measured Values of D_r for Different Random Step Sizes $\delta\theta$

$\delta\theta$	0.002	0.005	0.01	0.02	0.05
D_r	1.0×10^{-6}	0.65×10^{-5}	2.5×10^{-5}	1.0×10^{-4}	0.65×10^{-3}

The calculation in two dimensions is slightly more cumbersome but also leads to a behavior $\tau_n = \tau_a/n + \beta_1\tau_{rot} + (\beta_2 + \beta_3)\tau_{patch}$, with $\tau_a = 2\tau_{rot}\ln(a/r_C)$ Now, the domination of τ_a/n over $\beta_1\tau_{rot}$ is only logarithmic, and a deviation from the linear behavior of τ_n^{-1} with n is expected in all realistic cases, as implied by the exact result of eq 7 and shown in Figure 9.

As a conclusion, these qualitative arguments give the right scaling behavior of the mean reaction time but fail to predict prefactors such as 2 ln 2 in eq 14. They also predict the linearity of the inverse reaction time in the number of patches as well as the slow convergence to this linear regime in the case studied in section 2.2, corresponding to $n = 2$. The qualitative arguments do not account for the more complicated result in eq 13. We finally note that the rigorous approach of section 2, where the initial concentration of particles is fixed, leads naturally to the determination of the inverse reaction time (decay rate) τ^{-1}, whereas the qualitative electrostatic analogy, with a fixed reaction rate Q, rather gives reaction time τ.

3. Numerical Simulation of Reactions between Rotating Colloids

In this section, we numerically simulate the reaction−diffusion process that eventually leads two rotating colloids to bind. We will consider several different geometries similar to those described analytically in section 2. We assume as before that the two colloids are always kept close to each other as shown in Figure 2, which implies that the reactions are governed only by the rotational Brownian dynamics of the beads that we now describe.

The orientation of each colloid is characterized by a unit vector $\hat{z}$ that is a function of two angle parameters $\hat{z} \equiv (\theta, \phi)$ of the unit sphere, $\hat{z} \equiv (\sin\theta\cos\phi, \sin\theta\sin\phi, \cos\theta)$. The rotational Brownian dynamics of the colloids can be materialized by the random walk performed by $\hat{z}$ in its configurational space. One random step is defined by an infinitesimal rotation around the current orientation, and it is performed by adding a small fixed value $\delta\theta$ to angle θ and choosing a random value of angle ϕ: $0 \leq \phi \leq 2\pi$. Figure 1 shows one realization of the random walk performed by $\hat{z}$ on the unit sphere. The connection between the number of moving steps performed and the physical time t is provided by the rotational diffusion coefficient $D_r = \langle\theta(t)^2\rangle/4t$. We measure D_r for one colloid and several values of angular steps $\delta\theta$. Correlation function $f(p) = \langle\hat{z}(q+p)\cdot\hat{z}(q)\rangle$ is sampled every 1000 steps for a total duration of 10^6 random steps. By fitting the correlation function $f(p)$ with the expected shape $\exp(-2D_rp)$, we obtain D_r for the given step size. The measured values of D_r are shown in Table 1, and they obey $D_r = 0.25(\delta\theta)^2$. Below, we choose random step size $\delta\theta = 0.01$ that optimizes the rapidity of the simulations and the compactness of angular space exploration so that our simulations do not miss any of the possible reactions.

3.1. Reaction between One Colloid Carrying a Single Ligand and One or Two Colloids Saturated with Receptors. We first consider the case where one colloid carries a single ligand and the second colloid is fully saturated with receptors. In this limit, we perform only a simulation on the orientation of the colloid bearing the ligand. As explained before, a reaction occurs if the orientation vector is anywhere within the reaction patch defined by angle θ_C. The reaction time is proportional to the number of steps p_r required to bring the orientation vector

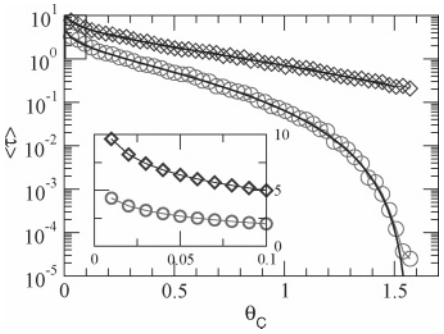

Figure 11. Average reaction time for a colloid carrying a ligand that reacts (i) with one colloid (◇) saturated with receptors as described in section 2.1 and (ii) with the two nearest neighbors in a chain of colloids (○), both saturated with receptors, as described in section 2.2. The solid lines are given, respectively, by eqs 5 and 8.

into the reaction patch, $\theta < \theta_C$. Its value will depend both on starting orientation $\hat{z}(p = 0)$ and on the particular random walk realization. Our simulations compute dimensionless average reaction times of $\langle\tau\rangle = \langle p_r D_r\rangle$ measured over 1000 different sets of initial random positions and different random walks. If the initial random orientation falls within the reaction patch, then the colloid reacts immediately, consistent with the assumptions in section 2.1. In particular, the dependence of the average reaction time on the patch size is expected under these conditions to follow eq 5.

We compute in a similar manner average reaction times for the situation where the colloid bearing the ligand is in a chain and can thus react with either of the two nearest neighbors in the chain. From the point of view of our simulation, we allow reactions to occur within reaction patches of angle θ_C located at both poles. In this configuration, the average reaction time is expected to follow eq 8 in section 2.2.

We plot in Figure 11 the average reaction time in units of D_r for simulations performed with $D_r = 2.5 \times 10^{-5}$ as a function of capture angle θ_C. The theoretical predictions (eqs 5 and 8) are shown as solid lines, and the symbols represent computed values from the numerical simulations. Symbols and lines show almost perfect agreement. As explained in section 2.2 and shown in Figure 9 for the longest relaxation time, the reaction between one colloid carrying one ligand and two saturated neighboring colloids is in practice 2 times faster that the reaction between a colloid with one ligand and one saturated colloid. The logarithmic corrections to the factor of 2 are due to the weak persisting correlations between events at opposite poles.

3.2. Reaction between One Colloid Carrying a Single Ligand and One Colloid Carrying More Than One Receptor. We consider in this section the reactions between two colloids, one colloid carrying a single ligand, and a second colloid bearing n receptors. The n receptors are randomly distributed over the surface of the colloid, with excluded volume radius $a = R\theta_S$, and the relative positions of the receptors are quenched.

We have argued in section 2.4 that the average reaction time for a reaction between one ligand and n receptors should scale as n^{-1} for systems where the average distance between reaction patches remains larger than the size of the patch (i.e., for colloids with a receptor surface coverage well below saturation). We plot in Figure 12 dimensionless reaction rate $\langle\tau\rangle^{-1}$ as we increase the number of receptors n with fixed reaction cone size θ_S. Each data point is an average over 500 different initial conditions for the ligand and receptors distributions. Because we expect that the reaction rate is in the linear regime a function only of the total

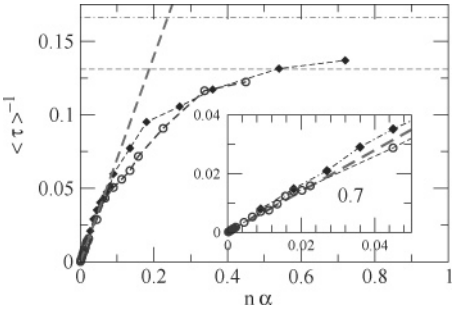

Figure 12. Reaction rate $\langle\tau\rangle^{-1}$ as a function of total receptor surface coverage $n\alpha$ for two different values of patch angles θ_C and θ_S: (i) (○) $\theta_C = \theta_S = 0.03$ and (ii) (◆) $\theta_C = \theta_S = 0.06$. The saturated values displayed in Figure 11 and predicted from eq 5 are represented by (○) a dashed line and (◆) a dotted-dashed line.

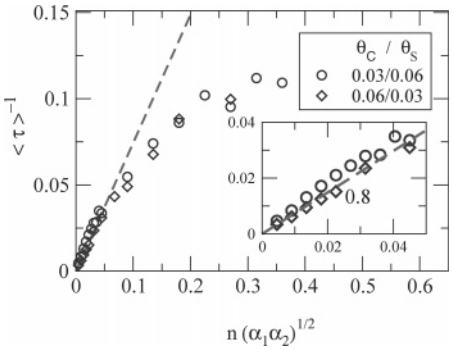

Figure 13. Reaction rate as a function of surface coverage of the streptavidins' asymmetric size of the reaction patch. ○ indicates 0.03 for biotin size and 0.06 for streptavidin, and ◇ is reversed biotin/streptavidin patch size.

coverage rate, the data is plotted against the combination $n(1 - \cos\theta_C)/2 = n\alpha$ that measures the relative surface covered by n patches.

As the Figure shows for two different reaction cone sizes $\theta_S = 0.03$ and 0.06, the reaction rate increases linearly with n and then crosses over to a saturating regime. The inset in the Figure shows that in the linear regime the two data sets collapse onto a single line of predicted slope $1/(2 \ln 2) \approx 0.7$ (eq 14). As the number of receptors increases, the reaction rates appear to approach the saturation values displayed in Figure 11 and predicted from eq 5. The simulation results indicate that the asymptotic limit is better reached by the smallest patches. Note, however, that the saturated case computed in section 2.1 is slightly different from the high-coverage limit in our simulations as a result of the unavoidable presence of nonreacting interstitial zones between the different reaction patches.

3.3. Asymmetric Reactions. When one considers reactions between ligands and receptors of arbitrary size, it might be convenient to allow for the flexibility of having different capture radii r_C for the ligand and r_S for the receptor that occupy different relative fractions α_C and α_S of the total colloid surface. We have shown in section 2.3 that the dimensionless average time $\langle\tau\rangle$ in this case is expected to vary as $\langle\tau\rangle = (\alpha_C\alpha_S)^{-1/2} g(x)$ with $x = (\alpha_C/\alpha_S)^{1/2}$ and $g(x)$ being the function $g(x) = (x + x^{-1}) \ln(x + x^{-1}) - (x - x^{-1}) \ln x$.

We plot in Figure 13 results for the reaction rate of asymmetric patch sizes. We consider two complementary cases, the first with $\theta_C = 0.03$ and $\theta_S = 0.06$ and the second with $\theta_C = 0.06$ and $\theta_S = 0.03$. Because $g(x)$ is invariant under the inversion of its argument $g(x) = g(x^{-1})$, the initial slopes of the rate curves should be the same if plotted as a function of $n(\alpha_C\alpha_S)^{-1/2}$. The Figure shows that this is indeed the case, and the obtained slope agrees well with the analytical predictions.

4. Conclusions

Recent progress[6,25] in the kinetic control of specific reactions between colloids carrying ligands and receptors calls for a rigorous theoretical description of the reaction diffusion mechanisms involved. The new techniques allow for the extraction of the actual time evolution of the reaction survival probability from experiments involving colloids bearing binding pairs with a tailored molecular architecture. The challenge is thus to develop a theoretical framework that is useful in connecting the observed reaction rates to the molecular characteristics of the biorecognition molecules. In this article, we considered reactions between two freely rotating colloids kept close to each other. This is the simplest model situation arising when magnetic beads are driven to form long chains by applied magnetic fields. For the bead size of interest in the experiments, the magnetic force constrains the average position of the bead centers but does not act on the rotational component of the Brownian motion.

Experimentally, all of the colloids carry a given number of receptors, and a small fraction of the beads carry one ligand. A reaction occurs when the ligand receptor pair comes within a reaction distance. Upon application of the magnetic field, the beads are brought into contact, and a reaction thus occurs when, by rotational diffusion, one ligand and one receptor align within some reaction angle. The value of this angle or correspondingly the value of the capture reaction radius is one of the molecular characteristics of the ligand receptor pair. For instance, when the two moieties are perfectly bound to the colloid surface, one requires alignment within a very small angle. A larger reaction patch will suffice if a spacer is used to tether either the ligand or the receptor to the surface.

We found that in all experimentally relevant situations the time required for a reaction to occur is larger than the characteristic rotational time of the diffusion motion τ_{rot}, a result that can be easily understood by the number of diffusion paths that do not intersect with the reaction patch. Quantitatively, the reaction time is determined by α, the relative surface occupied by the reaction patch $\alpha = \pi r_C^2/(4\pi r^2)$ where r_C is the capture radius and r is the radius of the colloid.

When the colloids are completely covered with receptors, only the diffusion of the ligand limits the reaction. In this asymptotic regime, the average reaction time $\langle\tau\rangle$ is larger than the rotation time τ_{rot} by only a logarithm factor of relative reaction surface α, $\langle\tau\rangle \simeq -\tau_{rot} \ln \alpha$. If the colloid carrying the ligand can react with either of the two neighbors in the chain, then the reaction time is reduced by roughly a factor of 2.

When the colloids carry only one receptor, the reaction−diffusion problem has a larger intrinsic dimension, and we find that the average reaction time has a stronger dependence on the value of the relative reaction surface, $\langle\tau\rangle \simeq \tau_{rot}(2 \ln 2)/\alpha$. The reaction time in this case is thus larger than that in the saturated case by a factor of $-2 \ln 2/(\alpha \ln \alpha)$

For most experimentally relevant situations, the colloids carry a finite number n of receptors. We found by analytical arguments and by numerical simulations that for small numbers of receptors the reaction time decreases inversely with the number of receptors (i.e., the reaction rate increases linearly with n). This linear behavior crosses over for large n to the value corresponding to saturation. We found numerically that linearity holds roughly over half of the time gap, so the linear variation with n is therefore valid up to $n \approx -2 \ln 2/(\alpha \ln \alpha)$.

Our predictions compare favorably with experimental results. In ref 25, the reaction time of 100 nm colloids of biotin/streptavidin pairs can be converted into a reaction patch size. For biotins and streptavidins firmly bound to the surface, a capture radius as small as a few angstroms is obtained, indicating the need for an almost perfect orientation of the colloids for the reaction to occur. If a spacer is introduced into the ligand, the receptor, or both, then the reaction times decrease correspondingly, a variation that can be quantitatively understood in terms of the patch size computed within our theoretical framework.

One of the important simplifying assumptions of our work is that the translational degrees of freedom associated with the Brownian motion of the center of the bead are irrelevant. This seems indeed to be the case in the experiments that inspired this work, but one can easily be confronted with situations where two neighboring beads need to overcome some repulsive potential in order to be in contact. The associated diffusion−reaction problem combines both rotational and translational diffusion. The theoretical and numerical techniques used in the present work are also well adapted to provide answers for the more complex situation.

A second simplifying assumption concerns the absence of hydrodynamic correlations between the two beads when they are within the reaction range. Although previous work[26] has shown that this is the case for model colloids at moderate distances, the presence of a stabilizing polymer corona could couple the Brownian motions of the two colloids. Accounting for such effects is an interesting theoretical challenge for a better understanding of the reaction dynamics in these systems.

Acknowledgment. N.-K.L. acknowledges KOSEF for financial support via grant F01-2005-000-10075-0. N.-K.L., A.J., F.T., and C.M.M. benefited from the CNRS/KOSEF exchange program "Adhesion Kinetics of Polymers and Membranes" under reference 20278.

Appendix A: An Alternative Solution of the Reaction Diffusion Equation for One Colloid Carrying a Single Ligand and One Colloid Saturated with Receptors

Equation 1 of section 2.1 can also be solved by the usual eigenmode expansion of the probability distribution

$$\psi(\theta, t) = \sum_{\nu_k} a_k P_{\nu_k}(-\cos\theta) \exp\left(-\frac{t}{\tau_k}\right) \qquad (33)$$

where P_ν is the Legendre function of the first kind and ν_k is the discrete eigenvalues obtained from $P_{\nu_k}(-\cos\theta) = 0$ and $1/\tau_k = \nu_k(\nu_k + 1)$ in units of τ_{rot}. Amplitudes a_k are extracted from the projection of $\psi(\theta, t = 0)$ into the base functions P_{ν_k}:

$$a_k = \frac{\int_{\theta_C}^{\pi} \sin\theta \, d\theta \, \psi(\theta, t = 0) \, P_{\nu_k}(-\cos\theta)}{\int_{\theta_C}^{\pi} \sin\theta \, d\theta (P_{\nu_k}(-\cos\theta))^2} \qquad (34)$$

It can be easily checked that for a patch angle $\theta_C = 0.3$, six modes are enough to give an accurate representation of the distribution probability, except at very short times where oscillations are still perceptible. The survival probability $\phi(t)$ has a corresponding form

(25) Cohen-Tannoudji, L.; Bertrand, E.; Baudry, J.; Robic, C.; Goubault, C.; Pélissier, M.; Johner, A.; Lee, N.; Thalmann, F.; Marques, C.; Bibette, J., Submitted for publication, 2007.

(26) Stark, H.; Reichert, M.; Bibette, J. *J. Phys.: Condens. Matter* **2005**, *17*, S3631−S3637.

$$\phi(t) = \sum_{\nu_k} b_k \exp\left(-\frac{t}{\tau_k}\right) \tag{35}$$

with the coefficients b_k given by

$$b_k = \frac{\int_{\theta_C}^{\pi} \sin\theta \, d\theta \, \psi(\theta, t=0) \, P_{\nu_k}(-\cos\theta) \int_{\theta_C}^{\pi} \sin\theta \, d\theta \, P_{\nu_k}(-\cos\theta)}{\int_{\theta_C}^{\pi} \sin\theta \, d\theta (P_{\nu_k}(-\cos\theta))^2} \tag{36}$$

For all practical purposes, the survival probability in the limit of small capture angles $\theta_C \ll 1$ is well approximated by the first term of the eigenfunction expansion (eq 35), and we show in Figure 14 the value of b_1 as a function of θ_C.

Appendix B: Alternative Solution of the Reaction Diffusion Equation for One Colloid Carrying a Single Ligand and Two Colloids Saturated with Receptors

The inverse Laplace transform of the probability distribution $\psi(\theta, s)$ in eq 6 of section 2.2 can also be obtained directly by an eigenmode expansion

$$\psi(\theta, t) = \sum_{\nu_k} a_k [P_{\nu_k}(-\cos\theta) + P_{\nu_k}(\cos\theta)] \exp\left(-\frac{t}{\tau_k}\right) \tag{37}$$

with ν_k in this case being the discrete eigenvalues obtained by solving $P_{\nu_k}(-\cos\theta) + P_{\nu_k}(\cos\theta) = 0$, and one also has $1/\tau_k = \nu_k(\nu_k + 1)$ in units of τ_{rot}. The amplitudes a_k are given by

$$a_k = \frac{\int_{\theta_C}^{\pi - \theta_C} \sin\theta \, d\theta \, \psi(\theta, t=0)[P_{\nu_k}(-\cos\theta) + P_{\nu_k}(\cos\theta)]}{\int_{\theta_C}^{\pi - \theta_C} \sin\theta \, d\theta [P_{\nu_k}(-\cos\theta) + P_{\nu_k}(\cos\theta)]^2} \tag{38}$$

The survival probability $\phi(t)$ follows a similar expansion

$$\phi(t) = \sum_{\nu_k} b_k \exp\left(-\frac{t}{\tau_k}\right) \tag{39}$$

with the coefficients b_k given by

$$b_k = \frac{\int_{\theta_C}^{\pi - \theta_C} \sin\theta \, d\theta \, \psi(\theta, 0)[P_{\nu_k}(-\cos\theta) + P_{\nu_k}(\cos\theta)] \int_{\theta_C}^{\pi - \theta_C} \sin\theta \, d\theta [P_{\nu_k}(-\cos\theta) + P_{\nu_k}(\cos\theta)]}{\int_{\theta_C}^{\pi - \theta_C} \sin\theta \, d\theta [P_{\nu_k}(-\cos\theta) + P_{\nu_k}(\cos\theta)]^2} \tag{40}$$

Figure 15 shows the decay of the value of amplitude b_1 of the survival probability as a function of θ_C. For most relevant purposes, the value can be taken as unity.

Appendix C: Accuracy of the Solution Obtained from the Propagator

The solution of a diffusion reaction equation can be obtained by solving a diffusion equation with the appropriate boundary conditions in only a limited number of cases. The cases treated in sections 2.1 and 2.2 for a reaction between one colloid carrying a ligand and one or two saturated colloids are among the rare examples where such a simple method can be applied. This simple method cannot be used, for instance, for the case solved in section 2.3 for one colloid with one ligand reacting to one colloid with one receptor. In these cases, a different method needs to be applied to extract the relevant physical information; this method often relies on decoupling approximations that we now discuss and validate.

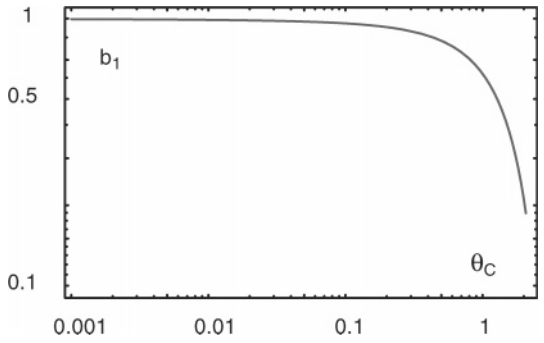

Figure 14. Variation of amplitude b_1 of the eigenfonction expansion of survival probability $\phi(t)$ as a function of capture angle θ_C.

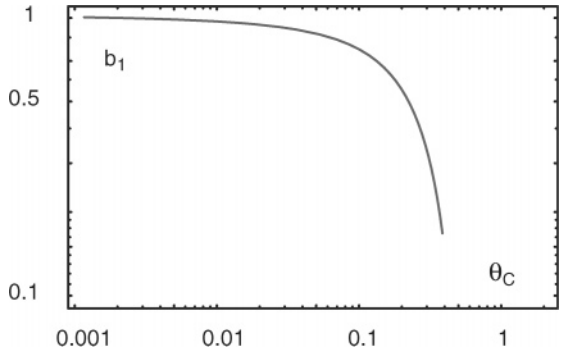

Figure 15. Variation of amplitude b_1 of the eigenvalue expansion of survival probability $\phi(t)$ as a function of the capture angle θ_C.

We discuss in this Appendix the accuracy of the so-called propagator-based solution to the reaction diffusion equation (eq 1). The solution is based on the formal rewriting of the differential equation (eq 1) as an integral equation

$$\psi(\theta, t) = \psi^{eq} - \int_0^t dt' \int_0^{\pi} \sin\theta' \, d\theta' \, G_0(\theta, \theta'; t - t') \, Q(\theta') \, \psi(\theta', t') \tag{41}$$

for the case where the reaction starts at time $t = 0$ from equilibrium distribution $\psi(\theta, t = 0) = \psi^{eq}$. $Q(\theta)$ describes the shape and rate of the reaction well, and $G_0(\theta, \theta'; t)$ is the propagator associated with the corresponding free-diffusion problem in the absence of reactions

$$\frac{\partial G_0(\theta, \theta'; t)}{\partial t} - \nabla_\theta^2 G_0(\theta, \theta'; t) = \delta(\theta - \theta') \, \delta(t) \tag{42}$$

that measures the probability of finding a particle at time t and angle θ, knowing that it was at angle θ' at time $t = 0$. The propagator can be computed either from the eigenmode expansion

$$G_0(\theta, \theta'; t) = \frac{1}{2} \sum_{m=0}^{\infty} P_m(\cos\theta) \, P_m(\cos\theta') \exp\{-D_{rot} \, m \, (m+1) t\} \tag{43}$$

with P_m being the usual Legendre polynomials, or from the equivalent Laplace-transformed form

$$G_0(\theta, \theta'; s) = -\frac{1}{2D_{rot}} \frac{\pi}{\sin \pi\nu(s)} P_{\nu(s)}(\cos\theta) \, P_{\nu(s)}(-\cos\theta') \tag{44}$$

with P_ν being the Legendre functions. The s-dependent index is computed from $\nu(\nu+1) = -s/D_{rot}$. Both forms assume an initial equilibrium distribution of $\psi^{eq} = {}^1/_2$.

When the reaction sink is represented by a delta function $Q(\theta) = q\delta(\theta - \theta_C)$, eq 41 assumes the simple time convolution form

$$\psi(\theta, t) = \psi^{eq} - q\int_0^t dt'\, G_0(\theta, \theta_C; t - t')\, \psi(\theta_C, t') \qquad (45)$$

that can be easily solved by Laplace transform and written as

$$\psi(\theta, s) = \frac{\psi^{eq}}{s}\left(1 - \frac{qG_0(\theta, \theta_C; s)}{1 + qG_0(\theta_C, \theta_C; s)}\right) \qquad (46)$$

In the limit of very fast local reactions, one can take the limit $q \to \infty$ to obtain an expression for the Laplace transform of the probability distribution identical to expression 2 in section 2.1. In this description of the reaction diffusion problem, the probability distribution holds for the whole angle domain $\theta \in [0, \pi]$ and vanishes only at the point $\theta = \theta_C$. The longest relaxation time of this problem is thus equivalent to the longest relaxation time of solution 2, but the survival probability $\phi(t)$ and the average time $\langle\tau\rangle = \int_0^\infty \phi(t)\, dt$ will, in principle, be different. Note however that the differences are only marginal in the limit of a very small capture radius.

When the reaction sink has a finite width, say $Q(\theta) = q$ for $0 \le \theta \le \theta_C$ and $Q(\theta) = 0$ otherwise, eq 41 does not reduce to a time convolution. However, a functional simplifying assumption can be made by noticing that for small reaction patches the propagator varies only slightly inside the reaction sink and one can thus write the time convolution equation

$$\psi(\theta, t) = \psi^{eq} - q\int_0^t dt'\, G_0(\theta, 0; t - t') \int_0^{\theta_C} \sin\theta'\, d\theta'\, \psi(\theta', t') \qquad (47)$$

and the corresponding solution for the probability distribution, here in the limit of $q \to \infty$

$$\psi(\theta, s) = \frac{\psi^{eq}}{s}\left(1 - \frac{G_0(\theta, 0; s)}{\int_0^{\theta_C} \sin\theta\, d\theta\, G_0(\theta, 0; s)} \frac{\int_0^{\theta_C} \sin\theta\, d\theta\, \psi^{eq}}{\psi^{eq}}\right) \qquad (48)$$

Inserting the explicit form (eq 44) for the propagator $G_0(\theta, 0; s)$ and the value of the equilibrium distribution $\psi^{eq} = {}^1/_2$ yields

$$\psi(\theta, s) = \frac{1}{2s}\left(1 - \frac{P_{\nu(s)}(-\cos\theta)}{\frac{1}{\int_0^{\theta_C} \sin\theta\, d\theta} \int_0^{\theta_C} \sin\theta\, d\theta\, P_{\nu(s)}(-\cos\theta)}\right) \qquad (49)$$

The expression above should also be compared with the Laplace transform of the probability distribution (eq 2) of section 2.1: the angular dependence is identical, and the longest relaxation time, given by the smallest pole of $\int_0^{\theta_C} \sin\theta\, d\theta\, P_\nu(s)(-\cos\theta)$, has a similar asymptotic dependence of $\tau_{long} \simeq \tau_{rot} \ln\alpha$ in the limit of small patches. The Laplace transform of the survival probability $\phi(s) = \int_{\theta_C}^{\pi} \sin\theta\, d\theta\, \psi(\theta, s)$ can be conveniently written as

$$\phi(s) = \frac{h(s)}{1 + sh(s)} \qquad (50)$$

where $h(s)$ is the Laplace transform of the relaxation function $h(t)$ given by

$$h(t) = \frac{\int_0^{\theta_C} \sin\theta\, d\theta\, G_0(\theta, 0; t)}{\int_0^{\theta_C} \sin\theta\, d\theta\, \psi^{eq}} - 1 \qquad (51)$$

As for previous cases, the survival probability here also has the longest relaxation time, obtained by solving $1 - (1/\tau_{long})h(-1/\tau_{long}) = 0$, identical to the relaxation time of the probability distribution, $\tau_{long} \simeq \tau_{rot} \ln\alpha$.

The previous study shows that for the case of one bead with one ligand and one bead saturated with receptors there are only marginal differences associated with the details of the reaction. Indeed, requiring that the reaction takes place exactly at $\theta = \theta_C$ or allowing for reactions anywhere inside the patch $\theta \le \theta_C$ leads essentially to the same reaction behavior in the relevant limit of small patches.

The situation for the case of one bead carrying one ligand and one bead carrying one receptor is rather different. We have considered in section 2.3 a reaction model based on the reaction function $Q(\theta_1, \theta_2) = q$ if ($0 \le \theta_1 \le \theta_C$ and $0 \le \theta_2 \le \theta_S$) and $Q = 0$ otherwise. Such a model states that a reaction occurs whenever the ligand and the receptor are simultaneously inside the reaction patch, centered at $\theta = 0$. This implies a decoupling approximation in the mathematical treatment of the solution, and one might wonder why the delta function, $Q(\theta_1, \theta_2) = q\delta(\theta_1 - \theta_2)$, that allows for an exact solution of the problem is not used. It can easily be shown, along the same lines of the calculations discussed in this Appendix, that the requirement of having both the ligand and the receptor at the same angular position is too stringent and leads to a divergent reaction time.

Appendix D: Electrostatic Analogy for Many Reaction Sites

We consider a collection of identical spherical reaction zones $\mathscr{R}_i$ in dimension d. We call σ_d the (hyper)area of a sphere of radius 1 so that the volume of a patch ν_{patch} reads $\sigma_d r_C^d/d$ and the total volume of the configuration space is $\nu_{conf} = \sigma_d a^d/d$. The electrostatic problem consists of finding the charges q_i borne by each conductor $\mathscr{R}_i$, then calculating the potential $V(\boldsymbol{\rho})$ generated between the conductors, and finally integrating this potential over the volume between the conductors.

When isolated, each site i creates a potential V_i

$$V_i(\rho_i) = \frac{q_i}{(d-2)\sigma_d}\left(\frac{1}{r_C^{d-2}} - \frac{1}{\rho_i^{d-2}}\right) \qquad (52)$$

where ρ_i stands for the relative distance from the center of $\mathscr{R}_i$. The average potential due to the other charges near $\mathscr{R}_i$ is

$$\delta V_i = \sum_{j\neq i, j=1}^{n} \frac{q_j}{(d-2)\sigma_d}\left(\frac{1}{r_C^{d-2}} - \frac{1}{r_{ij}^{d-2}}\right) = \delta V \qquad (53)$$

with r_{ij} being the mutual distance between $\mathscr{R}_j$ and $\mathscr{R}_i$. Because all the conductors must be simultaneously set equal to $V = 0$, shift δV_i cannot depend on index i. This is achieved by adjusting charges q_i, which now depend on the relative spatial arrangement of the reaction zones. In practice, the set of q_i must fulfill $n - 1$ linear constraints, leaving only one degree of freedom for the total charge $Q = \sum_{i=1}^n q_i$. Thus, in the limit $r_C \ll r_{ij} \approx a$, δV reads

$$\delta V = \frac{1}{n}\sum_{i=1}^{n}\delta V_i = \frac{n-1}{n}\frac{Q}{(d-2)\sigma_d r_C^{d-2}} - \frac{1}{2n}\sum_{i,j=1,i\neq j}^{n}\frac{1}{(d-2)\sigma_d}\frac{q_i+q_j}{r_{ij}^{d-2}}$$

$$= \frac{(n-1)}{n(d-2)\sigma_d}\frac{Q}{r_C^{d-2}} + \frac{C_2}{\sigma_d}\frac{Q}{a^{d-2}} \tag{54}$$

where the C_2 constant is of order unity and depends only on the relative spatial arrangement of the reaction sites. The resulting potential

$$V_{tot}(\rho) = \sum_i V_i(\rho_i) - \delta V \tag{55}$$

has the property that its spatial average value around any boundary $\partial\mathscr{R}_i$ is zero. In the equation, ρ represents any point outside the reaction zone. Because by assumption $V_i(r_C) = 0$ and because the potential created by the other charges is harmonic ($\Delta V = 0$), the average value of V_{tot} at boundary $\partial\mathscr{R}_i$ coincides at the lowest order with its value at the center of $\mathscr{R}_i$, and shift $-\delta V$ ensures that it vanishes for all sites $\mathscr{R}_i$. This holds because by assumption the size of the patches is small compared to the inter-patch distances. The only deviations to the equipotential condition $V = 0$ are anisotropic and correspond to the mutual polarization effect discussed below. Then, the total number of particles N is given by the integration over all configuration space of the total potential ν_{tot}. The integration of all of the constant terms lead to a common factor $\nu_{tot} - n\nu_{patch}$ representing the total volume, exclusive of the n reaction zones. The integration of the nonconstant terms (power law ρ_i^{-d-2}) presents no difficulty, but again, care must be taken to remove the excluded volume contributions. As a result, we find that in d dimensions, $d \geq 3$,

$$N = \frac{Q}{D_t}\left\{\frac{1}{n(d-2)}\frac{a^d}{r_C^{d-2}} + B_1 a^2 + B_2 r_C{}^2\right\} \tag{56}$$

with B_1 and B_2 being two constants of order unity, and

$$\tau_n = \frac{\tau_a}{n} + \beta_1\tau_{rot} + \beta_2\tau_{patch} \tag{57}$$

with $\beta_1 = 4B_1$, $\beta_2 = 4B_2$, $\tau_{rot} = a^2/4D_t$, and $\tau_{patch} = \tau_{rot}r_C{}^2/a^2$ where τ_a is the leading asymptotic time corresponding to a single capture site

$$\tau_a = \frac{4}{d-2}\frac{a^{d-2}}{r_C^{d-2}}\tau_{rot} \tag{58}$$

Let us evaluate the polarization corrections. In dimension d, the field generated by a conductor i is $E_d(\rho_i) = q_i\rho_i^{-(d-1)}/\sigma_d$, and the polarization gained by the second conductor is the product of the electric field and the total volume (polarizability) σ_d/dr_C^d of the conductor: $P_{ij} = \sigma_d E_d(r_{ij})r_C^d/d$. This reaction potential is about $P_{ij}r_{ij}^{-(d-1)}$ near the first conductor. This typically shifts the potential by another amount $\delta V'$

$$\delta V' = Qr_C^d a^{2-2d} \tag{59}$$

and the reaction time is modified by an extra $\beta_3\tau_{patch}(r_C/a)^{d-2}$, which is negligible for $d \geq 3$.

The calculation in two dimensions can be made in a similar way, with some extra care due to the nondecreasing behavior of $V_i(\rho_i)$ at large ρ_i. We find that the potential shift δV reads

$$\delta V = \frac{(n-1)Q}{2\pi n}\ln\left(\frac{a}{r_C}\right) + \sum_{i,j=1,i\neq j}^{n}\frac{q_i+q_j}{2\pi}\ln\left(\frac{r_{ij}}{a}\right)$$

$$= \frac{(n-1)Q}{2\pi n}\ln\left(\frac{a}{r_C}\right) + QC_2 \tag{60}$$

where C_2 is again on the order of unity and independent of the patch size.

Our total population N reads

$$N = \frac{Q}{D_t}\left\{\frac{a^2}{2n}\ln\left(\frac{a}{r_C}\right) + B_1 a^2 + B_2 r_C{}^2\right\} \tag{61}$$

and the reaction time is

$$\tau_n = \frac{\tau_a}{n} + \beta_1\tau_{rot} + \beta_2\tau_{patch} \tag{62}$$

with $B_2 = (n-1)/(2n)\ln(a/r_C) + {}^1/_4$ and $\beta_2 = 4B_2$ being constants of order $\ln(a/r_C)$ or unity, B_1 is a first-order constant, $\tau_{rot} = a^2/4D_t$, $\tau_{patch} = \tau_{rot}r_C{}^2/a^2$, and $\tau_a = -\tau_{rot}\ln(\alpha)$. Now, the domination of term τ_a/n over $\beta_1\tau_{rot}$ is only logarithmic. Finally, in two dimensions, the polarization corrections lead to another term $\beta_3\tau_{patch}$, which, except for the logarithm $\ln(a/r_C)$, compares with $\beta_2\tau_{patch}$.

We conclude that the electrostatic analogy supports our numerical findings concerning the reaction rate as a function of the surface coverage, presented in Figures 12 and 13. With an effective dimensionality of $d = 4$ and a ratio r_C/a of order $\theta_s/2\pi \geq 0.01$, it is not surprising that the linear behavior of the reaction rate with n holds.

LA701639N